Polygonal model for layered inorganic nanotubes

Kevin Tibbetts,* Robert Doe,† and Gerbrand Ceder‡
Department of Materials Science and Engineering, Massachusetts Institute of Technology, Cambridge, Massachusetts 02139, USA
(Received 7 January 2009; published 8 July 2009)

Multiwalled inorganic nanotubes with circular cross sections must have either an incoherent interface or a large amount of strain. However, nanotubes with a polygonal cross section can have a coherent interface with considerably less strain. We present a model for polygonal nanotubes with no defects where the chirality of the nanotube determines the shape of the cross section. Circular and polygonal nanotubes are compared based on their strain energy and interfacial energy. We have used first-principles calcuations to parameterize strain and interfacial energy for TiS_2 nanotubes. These calculations show that the polygonal model is energetically favorable to the circular model when the inner radius is above a critical radius, 6.2 Å for a TiS_2 nanotube with ten layers. These results should provide insight into further investigations of nanotube structure and allow computational studies to more accurately predict nanotube properties.

DOI: 10.1103/PhysRevB.80.014102 PACS number(s): 61.46.Np, 71.15.Mb

I. INTRODUCTION

Following the discovery of carbon nanotubes in 1991[1] many noncarbon materials have also been synthesized in nanotube form.[2–9] The rich chemical variety of such inorganic nanotubes may lead to substantial opportunity for tuning materials properties. In this manuscript we develop a general model for the structure of multiwalled inorganic tubes.

Nanotubes can be synthesized from layered (two dimensional) or nonlayered (three dimensional) materials. Carbon nanotubes as well as most inorganic nanotubes prepared to date are layered nanotubes.[1–4] In general, layered nanotubes consist of the same layers that the bulk material is comprised of, rolled into a tubular form. Nonlayered nanotubes are typically made by growing the material in a template with nanosized pores.[10,11] If growth is stopped before the pores are filled, nanotubes are the result, while if the pores are filled, nanowires are created. In this paper we will focus on layered nanotubes.

Layered nanotubes can be single walled[12–15] or multiwalled.[1–4] In some cases these nanotubes are nanoscrolls,[16–18] or jelly roll nanotubes, meaning one layer is scrolled to form a tube (the cross section is a spiral). In other cases the multiwalled nanotube consists of several concentric "single-walled" nanotubes.[2,19,20] In this paper we develop a model for the energy and shape of concentric, multiwalled nanotubes, but the main ideas can likely also be applied to nanoscrolls.

In layered nanotubes there is a single sheet that is considered the basic structural unit of the nanotube. For carbon nanotubes this sheet is a single atomic layer, known as graphene. For boron nitride (BN) nanotubes, first discovered in 1995,[21] the basic unit is the same single atomic layer sheet as for carbon nanotubes with carbon atoms replaced by Boron and Nitrogen. The majority of inorganic layered nanotubes are of the form MX_2 (M=transition metal, X=S, Se, O). The basic structural unit for these nanotubes is a triple layer sheet, consisting of a layer of transition metal cations sandwiched between layers of anions. WS_2 nanotubes were the first MX_2 nanotubes discovered in 1992,[2] soon followed by MoS_2 nanotubes in 1993.[3] Numerous other materials of the form MX_2 have shown stability in tubular form.[5–9]

Many applications for inorganic nanotubes have been discovered. WS_2 nanotubes have proven to be effective solid lubricants,[22] display shock-wave resistance[23] and have been used as tips in scanning probe microscopy.[24] TiO_2 nanotubes have been used as hydrogen sensors,[25] dye sensitized solar cells,[26] and have displayed photoluminescence properties.[27] Many inorganic layered nanotubes have shown the ability to intercalate lithium, hydrogen, and magnesium,[28–37] indicating potential as energy storage materials.

In this paper we present a model for multiwalled nanotubes with a polygonal-cross section and parameterize it with first principles calculations for TiS_2. A polygonal nanotube has more strain energy than a circular tube, due to a decrease in radius of curvature at its corners, but in return has less interfacial energy. There is evidence of multiwalled carbon[20,38–41] and boron nitride[42,43] nanotubes with a polygonal-cross section. The existence of graphitic polyhedral crystals has been known for many years.[44–47] These are large tubes where the core has a circular-cross section and the shell has a polygonal-cross section. Multiple studies have shown that bundles of single-walled carbon nanotubes will develop a polygonal-cross section when subjected to hydrostatic pressure.[48–51] Among dichalcogenides, there is evidence of polygonal WS_2 nanotubes.[52,53] There have been several computational studies of polygonal carbon nanotubes.[51,54–56] Theories on the structure of polygonal nanotubes typically assume that defects form at the polygon corners.[39,41]

Using our model, we find that for reasonable tube diameters a tube can lower its energy by forming a polygonal-cross section where the only defects are stacking faults. The optimal shape of the polygon, specifically the number of sides, depends on the interlayer spacing and the chirality of the nanotube. In Secs. II and III, we explain the polygonal model and discuss the various energy components of this model. In Sec. IV, we present the computational and structural details of our calculations. In Sec. V, we explain the results of the calculations and in Sec. VI we discuss some additional considerations of the polygonal model.

II. ENERGY COMPONENTS OF NANOTUBES

Because the length of nanotubes is considerably larger than their diameter they can be considered infinite along the tube axis. In our calculations the unit cell consists of the complete cross section of the nanotube with a length along the nanotube axis defined by some multiple of the periodic distance in this direction. Calculations discussed in this paper are for armchair (n,n) nanotubes with a periodic unit along the nanotube axis of 3.46 Å. Nanotube energies discussed in this paper refer to this periodic unit, unless specifically designated as energy per atom. The diameter of inorganic nanotubes seen experimentally is approximately 10 nm.[2,57–59] The periodic unit cell of a single layer tube with this diameter contains approximately 315 atoms. Two layers (630 atoms) are required to determine the structure and interaction between layers. First principles calculations are impractical for this many atoms so calculations on complete nanotubes of this size are not performed.

An alternative to the explicit calculation of large tubes is to divide the energy of a nanotube into a number of energy components and analyze the components separately. The energy of a nanotube, relative to the bulk material, can be divided into four components: strain energy, interfacial energy, defect energy, and surface energy. The total energy of the nanotube can thus be written as,

$$E_{\text{Total}} = N\epsilon_{\text{bulk}} + E_{\text{strain}} + E_{\text{interface}} + E_{\text{defect}} + E_{\text{surface}}. \quad (1)$$

In this equation N is the number of atoms, ϵ_{bulk} is the bulk energy per atom, and all other energy terms represent the excess energy of the nanotube due to various components. In this paper we compare the energy of two possible structures for nanotubes, a polygonal model in which the sides of the tube form polygonal faces, and a more cylindrical model in which the tube cross section is circular. The surface energy per unit area for each of these models will be approximately identical so this component is not important. Defect formation is an important energetic component that can affect the structure of a nanotube. Defects could lower the energy of polygonal nanotubes, increasing the likelihood of their formation, however their treatment lies outside the scope of the work presented here. The two energy components discussed in detail in this paper are the strain energy and interfacial energy.

A. Strain energy

1. Bending strain energy

The bending strain energy is the energy required to apply a given amount of curvature to a sheet of material. In linear elasticity the bending strain energy per atom, ϵ_{bend}, is inversely proportional to the square of the radius of curvature, r_c. The number of atoms, N, in a circular nanotube cross section with the periodic length is proportional to the radius of curvature (radius of the circle) so the total bending strain energy, E_{bend}, is inversely proportional to the radius. This can be shown mathematically as:

$$\epsilon_{\text{bend}}(r) = \frac{C_{\text{bend}}}{r^2}, \quad (2)$$

$$N(r) = 2\pi \times C_{\text{length}} r, \quad (3)$$

$$E_{\text{bend}}(r) = N\epsilon_{\text{bend}} = \frac{2\pi C_{\text{length}} C_{\text{bend}}}{r}, \quad (4)$$

where C_{bend} is the bending strain energy constant and C_{length} is a factor to convert from length to number of atoms. These two constants, C_{bend} and C_{length}, are independent of the radius of curvature and depend only on the material.

2. Tensile strain energy

Tensile strain energy is the energy required to stretch or compress a sheet of material. Stretching or compressing of nanotube layers is often necessary in order to achieve a coherent interface between layers. Tensile strain is defined by the strain fraction, ϵ, which is the ratio of the change in length, Δl, to the initial length, l_0.

$$\epsilon = \frac{\Delta l}{l_0}. \quad (5)$$

Tensile strain energy per unit volume is proportional to the square of the strain fraction, with the constant of proportionality equal to one half of the Young's Modulus.

$$E_{\text{tensile}} = N_\epsilon U_0 \frac{E}{2}\epsilon^2 \quad (6)$$

In Eq. (6), N_ϵ is the number of atoms under tensile strain, U_0 is the volume per atom and E is Young's Modulus.

B. Interfacial energy

The interfacial energy component corresponds to the energy of an incoherent interface relative to a coherent interface. The interface between two layers of a multiwalled nanotube cannot be coherent without the inclusion of tensile strain, due to the difference in the circumference of consecutive layers. When the interface is coherent, the same number of unit cells has to be spread out over a length that increases with distance from the center of the nanotube. This is unlikely for multiwalled tubes due to the large amount of strain required. Figure 1 is a simple representation of two layers of TiS_2 where the blue dots represent Ti atoms (S atoms are not shown for ease of viewing). Figure 1(a) shows two flat layers, analogous to the bulk where Ti atoms in one layer project directly above Ti atoms in a preceding layer. No strain is required to maintain alignment throughout the layers. Figure 1(b) shows two of these layers bent independently of each other, with the radii of curvature of the two layers analogous to consecutive layers in a nanotube. In order for the interface to be coherent, the alignment lines should be perpendicular to the surface. While this is true in the center of Fig. 1(b), for most of the nanotube the difference in length between the two layers results in an incoherent interface. Figure 1(c) shows two layers bent with the same curvature as in Fig. 1(b), but the layers are strained so as to maintain the bulk alignment. In this figure the alignment lines are perpendicular to the surface. However, a large amount of tensile strain is required to achieve this alignment.

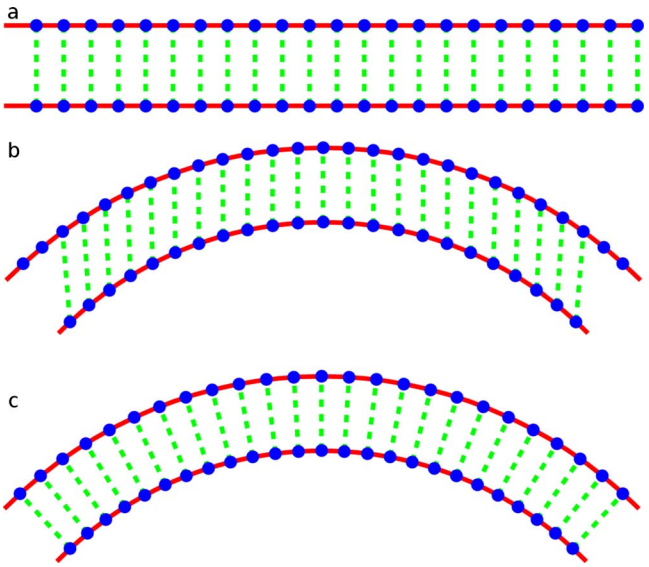

FIG. 1. (Color online) Alignment diagram. Bulk alignment (a) cannot be maintained when layers are curved without strain (b). If tensile and compressive strain is applied (c) bulk alignment can be maintained

The tensile strain energy required to maintain this alignment for multiple layers grows rapidly with the number of layers ($E_{\text{tensile}}\alpha n^3$).

The interfacial energy term in Eq. (1) is defined as the binding energy of a coherent interface minus the binding energy of an incoherent interface. This can be represented by an interfacial energy constant, γ_{int}, which gives the interfacial energy per unit of interfacial area.

$$E_{\text{interface}} = E_{\text{incoherent}} - E_{\text{coherent}} = N_{\text{inc}} A_0 \gamma_{\text{int}}. \tag{7}$$

In this equation, N_{inc} is the number of atoms with an incoherent interface and A_0 is the interfacial area per atom.

III. NANOTUBE MODELS: POLYGONAL VERSUS CIRCULAR-CROSS SECTION

We will compare the energy of a normal cylindrical tube with that of a polygonal tube. The polygonal model discussed in this paper consists of nanotubes where the cross section is a polygon with rounded corners. The bending strain energy is localized to the corners of the polygon, resulting in increased strain energy, but the flat sides of the polygon provide a coherent interface leading to a reduction in interfacial energy. Because the interfacial energy is much larger than the bending strain energy the polygonal model can often result in lower overall energy than that for a nanotube with a circular-cross section. In this section we will first discuss the polygonal model in relation to single-walled nanotubes, and then we will expand this to multiwalled tubes and explain what determines the number of sides to the polygon.

A. Single polygonal tube

In an ideal polygon the corners are perfectly sharp, i.e., the radius of curvature of the corners is 0. This is not practical for a nanotube. The corners will have some finite radius of curvature, which will define the strain energy of the nanotube. To illustrate this point Fig. 2(a) depicts a six-sided polygon with the radius of curvature labeled. All of the strain energy is localized in these curved corners; the flat sections are free of strain. The total strain energy of a single polygonal tube depends only on this radius of curvature. To prove this point, consider an N-sided polygon. This polygon will have N corners, each with the same radius of curvature, r_c, and subtending an angle of $\frac{2\pi}{N}$. The length of the strained arc at each corner is thus $\frac{2\pi}{N} r_c$. Therefore, the total strain energy per unit cell for this tube will be:

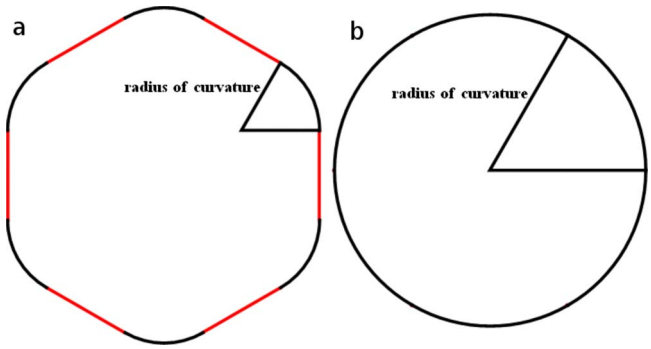

FIG. 2. (Color online) Bending strain in a single-walled polygonal nanotube (a) is localized to the corners where the radius of curvature is less than that of a cylindrical nanotube (b) with equal circumference

$$E_{\text{bend}} = N C_{\text{length}} \frac{2\pi}{N} r_c \frac{C_{\text{bend}}}{r_c^2} = \frac{2\pi C_{\text{bend}} C_{\text{length}}}{r_c} \tag{8}$$

The total strain energy is independent in the number of sides and only depends on the radius of curvature at the corners. Equation (8) is equivalent to Eq. (4) for bending strain energy with the radius of the tube replaced by the radius of curvature at the corners. For a single-walled nanotube there is no interfacial energy so the optimum structure is the one that minimizes the bending strain energy, which occurs for the maximum radius of curvature. For a given number of atoms on the circumference, the maximum radius of curvature results in a circle, Fig. 2(b).

B. Multiwalled tube

For a multiwalled nanotube the polygonal model provides lower interfacial energy than a circular nanotube as the flat sections of the tube can be coherent and without strain, although this occurs with an increase in strain energy due to the smaller radius of curvature in the corners. All of the incoherence and strain is localized in the corners of the polygon. Figure 3 shows two consecutive nanotube layers where the thick red lines represent a coherent interface. The outer layer has more length and thus more atoms than the inner layer. When the cross section is circular, as in Fig. 3(a), these excess atoms are spread evenly around the circumference of the tube, resulting in a mostly incoherent interface. When the cross section is a polygon [Fig. 3(b)] it is possible for the flat sections to have a coherent interface as all of the excess

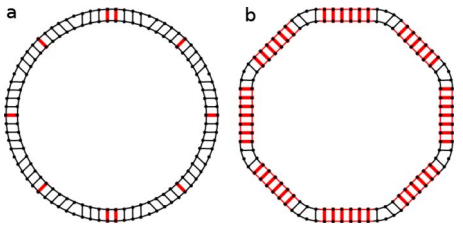

FIG. 3. (Color online) Multiwalled (a) cylindrical nanotubes have less coherent interface than (b) polygonal nanotubes. Thick red lines represent coherent interface while black lines represent incoherent interface.

atoms are located in the corners of the polygon.

A nanotube with n layers will have $n-1$ interfaces and its energy per unit cell can be obtained by adding the strain and interfacial energy

$$E = n \times \frac{2\pi C_{\text{bend}} C_{\text{length}}}{r_c} + (n-1)2\pi r_c l_{\text{unit}} \gamma_{\text{int}}, \tag{9}$$

where γ_{int} is the interfacial energy per unit area and l_{unit} is the length of the unit cell. To simplify the equation, we assumed that the radius of curvature remains constant from layer to layer, which may not be the case. This will be discussed further in Sec. VI. To determine the optimum radius of curvature we minimize Eq. (9) with respect to the radius of curvature.

$$\frac{\partial E}{\partial r_c} = (n-1)2\pi l_{\text{unit}} \gamma_{\text{int}} - n\frac{2\pi C_{\text{bend}} C_{\text{length}}}{r_c^2} = 0, \tag{10}$$

$$r_c = \sqrt{\frac{n}{n-1}\frac{C_{\text{bend}} C_{\text{length}}}{l_{\text{unit}} \gamma_{\text{int}}}}. \tag{11}$$

One requirement of this model is that a coherent interface is attained on either side of each rounded corner. For this to occur, the difference in the length for two consecutive layers to go around one corner must be equal to an integer number of lattice vectors in the rolling direction. Figure 4 is a diagram of two consecutive layers to illustrate how the two layers must be coherent at the end of the curved segment.

The outer layer has additional length equal to $2\Delta l$, determined by the interlayer spacing, d, and the angle of the corner, β

$$\Delta l = d\tan\left(\frac{\beta}{2}\right) = d\tan\left(\frac{\pi}{N}\right). \tag{12}$$

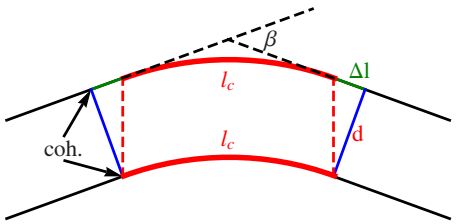

FIG. 4. (Color online) Two layers of a polygonal nanotube, representing the length difference between layers, δl, the curved length l_c, and the bending angle, β

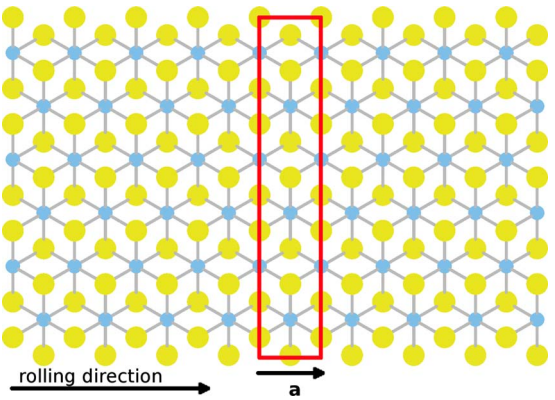

FIG. 5. (Color online) Top view of TiS_2 sheet showing the lattice vector in the rolling direction

In order for the layers to have a coherent interface at the points indicated, this excess length must equal an integer number of lattice vectors in the rolling direction. The lattice vector in the rolling direction is determined by the chirality of the nanotube. To illustrate this, Fig. 5 shows the top view of a TiS_2 sheet. The rolling direction indicated in the figure is that for a zigzag $(n,0)$ nanotube. The vector, a, is the lattice vector in the rolling direction.

This chirality dependence is the main restriction of the polygon model. There are only a few chiralities for which coherence of the flat segments can be achieved. For example, in TiS_2 the interlayer spacing, d, is equal to 5.7 Å. The total difference in length between consecutive layers is $2\pi d = 35.8$ Å. This length difference is divided evenly among the corners in the polygon model. As a result, there are only four chiralities (along with symmetric equivalents) that have a lattice vector small enough for the polygon model to apply. However, the symmetric equivalents constitute 38% of all possible nanotube chiralities. Table I lists the four chiralities. The first column, chirality, is the x,y vector defining the rolling direction, followed by a, the length of the lattice vector in the rolling direction, as shown in Fig. 5. The third column, β_{opt}, is the optimum bending angle for that lattice vector. The bending angle is illustrated in Fig. 4. N is the number of sides on a polygon with a bending angle that comes closest to β_{opt}. Next is the actual bending angle, β, corresponding to a polygon with N sides. The last column is the strain, ϵ, resulting from the difference between the lattice vector, a, and the excess length for the actual bending angle. The strain is this difference divided by the length of the curved segment, calculated for a radius of curvature of 14.7 Å. For all chiralities that are not a symmetric equivalent of one of the chiralities shown in Table I the polygon model will not apply, unless defects are included to provide the appropriate difference in length between layers. It is possible that the difference in length between successive layers going around the corner is not a full lattice vector, but instead results in a stacking fault in the flat section of the tube.

IV. CALCULATION DETAILS

A. Methodology

Calculations were carried out using density-functional theory (DFT) as implemented in the Vienna *ab initio* simu-

TABLE I. Allowed chiralities in the polygonal model as applied to TiS_2 nanotubes. For each chirality the table shows the length of the vector, maximum number of sides, angle of each corner and strain required at the corners of the polygon.

Chirality	a (Å)	β_{opt}	N	β	ϵ
1,0	3.460	34.780°	10	36°	−0.95%
2,1	5.993	60.240°	6	60°	0.11%
3,1	9.154	92.018°	4	90°	0.63%
4,1	12.475	125.399°	3	120°	1.26%

lation package (VASP).[60] We have used the generalized gradient approximation (GGA) of Perdew-Burke-Ernzerhof (PBE) to treat the exchange and correlation interaction. Projector augmented wave (PAW) potentials were used[61,62] with valence states $3d_3 4s_1$ for Ti and $3s_2 2p_4$ for S.

Structural parameters for a TiS_2 sheet, consisting of a sulfur-titanium-sulfur triple layer, were optimized using a three atom unit cell with a 15 Å vacuum layer. Atomic positions as well as unit cell shape and volume for this structure were relaxed using a $15\times15\times4$ Monkhorst-pack k-point mesh until the forces on all atoms were less than 0.03 eV/Å. The cell parameters determined for a TiS_2 sheet were used to create all curved surfaces examined in this study.

Bending strain was calculated using the curved surface method discussed in Refs. 63 and 64. These surfaces contain flat and curved sections as would occur in a polygonal nanotube. Interfacial energy calculations were made on structures containing two curved surfaces separated by the experimentally measured interlayer distance of 5.7 Å. The length of the curved segment was varied in order to vary the amount of incoherent interface.

When relaxing a curved surface, its size and shape were fixed by freezing the atomic positions of all Ti atoms; only the atomic positions of the S atoms were allowed to change. Inspection of the forces on the Ti atoms showed that freezing the Ti atoms did not have a significant effect on the results. Calculations were converged until all forces were less than 0.03 eV/Å with a gamma point centered k grid of $1\times1\times6$.

B. TiS_2 structure

We chose TiS_2 nanotubes for our study because they are a common type of inorganic nanotube and have potential as an energy storage material.[28–32,63] Bulk TiS_2 has long been studied as an intercalation compound and TiS_2 nanotubes have shown the ability to store hydrogen and lithium. Bulk TiS_2 forms the CdI_2-1T structure which consists of layers of Ti atoms octahedrally coordinated by S atoms.[63,65,66] These triple layers (S-Ti-S) are separated by a Van der Waals gap and stacked such that the titanium atoms project on top of each other. This triple layer is the basic structural unit of TiS_2 layered nanotubes.

V. RESULTS

A. Bending strain energy

The curved surface method was used to determine the bending strain energy constant for a triple layer of TiS_2. Calculations were performed on structures with various bending angles and curved lengths. Figure 4 shows the bending angle, β, and the curved length, l_c. These two parameters define the radius of curvature, $r_c=\frac{\beta}{l_c}$. The bending strain energy per formula unit is given by $\frac{C_{bend}}{r_c^2}$. The only unknown parameter in the equation for the bending strain energy (Eq. (8)) is the constant, C_{bend}.

In order to determine the bending strain energy constant we calculated the strain energy for structures with bending angles of 10, 20, 30, 40, and 60°. For each of these angles we performed calculations on structures with curved lengths of 10 and 20 Å. Figure 6 shows the results of these calculations. The points are the actual calculated strain energy, while Eq. (8) is plotted with a bending strain energy constant of 4.033 eV Å^2 per atom for the two different curved lengths. The data points agree with the fit line with an RMS deviation of 4.1 meV.

B. Interfacial energy

In layered structures such as TiS_2, the layers are held together by Van der Waals forces, which are not captured with DFT. However, when the stacking is disordered the distance between S atoms in consecutive layers is considerably less than the distance between S atoms in the same layer. The effect of this decrease in bond length, which is captured well with DFT, is a large contributor to the interfacial energy in this material due to the ionicity of the S-S interaction.[67] The interfacial energy will change with a change in interlayer spacing, but this was not investigated in this work, because it would be more strongly affected by Van der Waals forces and thus not accurately captured with DFT.

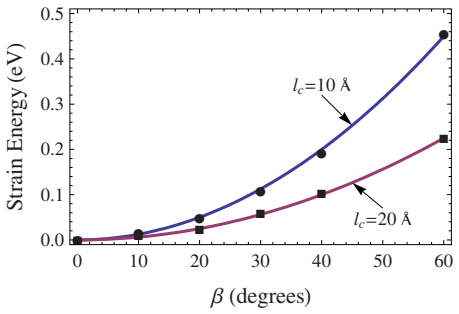

FIG. 6. (Color online) Strain energy versus bend angle for TiS_2 sheets with curved lengths of 10 and 20 Å

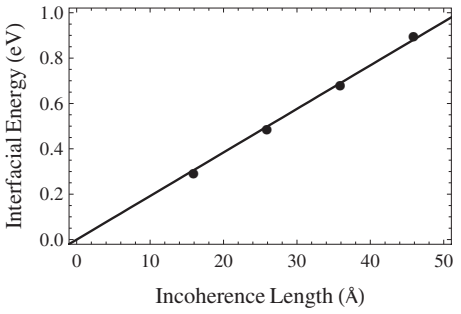

FIG. 7. Calculated Interfacial energy versus incoherence length for TiS_2 sheets

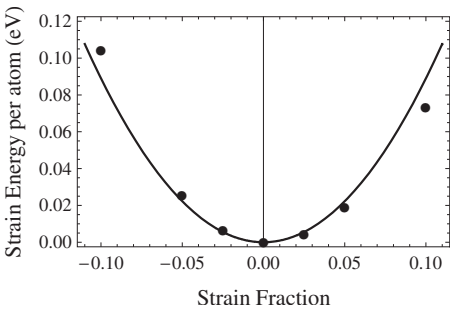

FIG. 8. Tensile strain energy of TiS_2 plotted versus strain fraction

To determine the interfacial energy for incoherent interfaces we created double layer curved surfaces consisting of two TiS_2 triple layers separated by 5.7 Å, the experimentally measured interlayer spacing in both bulk TiS_2 and TiS_2 nanotubes.[59] The length of the curved portion of these surfaces was varied in order to vary the amount of incoherent interface. Calculations were also performed on two flat TiS_2 triple layers separated by 5.7 Å to determine the energy of a completely coherent interface. The difference between the energy of two single layers and that of a double layer is the interfacial energy. The interfacial energy for the structure with a completely coherent interface is subtracted from the interfacial energy for the structures with some incoherent interface to give the excess energy due to an incoherent interface.

Figure 7 shows the excess energy plotted versus the amount of incoherent interface. The line fitted to the data corresponds to an interfacial energy constant of 18.67 meV per atom. This is the energy of an incoherent interface relative to a coherent interface. Structures with a different incoherence length also have a different radius of curvature and thus the structure of the interface is slightly different. The good agreement of the data points with the line indicate that the interfacial energy at the corners of the polygon can be well approximated by a single interfacial energy constant.

C. Tensile strain energy

The energy required to compress or expand a nanotube layer was not included in the previous equations, but it is a relevant factor in the overall energy of the polygonal model. Due to Hookes law this energy varies with the square of the strain fraction, ϵ. To determine the tensile strain energy constant, we made calculations on bulk TiS_2 with varying levels of compression and expansion of one of the in-plane lattice constants. The expected form of the results of these calculations was shown in Eq. (6). The results of these calculations are shown in Fig. 8. The data is fitted to Eq. (6) with a Young's modulus of 36.2 GPa, corresponding to a tensile strain energy constant, C_{tensile}, of 8.9 eV per atom.

VI. DISCUSSION

In the previous section we showed results that can be used to estimate the interfacial energy constant and the bending strain energy constant of TiS_2 and determine the nanotube shape with the lowest energy. Based on these results the low-energy radius of curvature for a polygonal nanotube can be calculated. Equation (11), repeated here, gives the optimum radius of curvature for a given number of layers, n.

$$r_c = \sqrt{\frac{n}{n-1}\frac{C_{\text{bend}}C_{\text{length}}}{l_{\text{unit}}\gamma_{\text{int}}}}. \tag{13}$$

Table II lists the two energy constants and the optimum radius of curvature for several values of the number of layers, n.

Based upon our model, when the radius of curvature at the corners of a polygonal nanotube is equal to the nanotube radius the cross section will be circular, because the entire circumference of the nanotube is taken up by the curved corners. For example, Table II shows that the optimum r_c is 20.79 Å when there are 2 layers in a TiS_2 nanotube, so when this nanotube exhibits a 2.079 nm radius both morphologies are identical in our model. More importantly, when the radius of the bilayer TiS_2 tube is less than 2.079 nm the circular-cross section is more favorable while radii greater than 2.079 nm should yield a polygonal-cross section. To generalize, multiwalled nanotubes exhibiting a radius smaller than the optimum radius of curvature (for a particular n value) should display circular-cross sections while nanotubes of radii greater than the optimum r_c should form a polygonal-cross section to yield a lower overall energy by creating straight segments. Equation (13) is derived from the approximate energy model for polygonal nanotubes shown in Eq. (9). In this section we will discuss some of the approxi-

TABLE II. Optimum radius of curvature, r_c, of the innermost nanotube layer decreases with the number of layers, n

Bending strain energy constant, C_{bend}	4.033 eV∗Å^2
Interfacial energy constant, γ_{int}	18.67 meV
$n=24$	$r_c=20.79$ Å
$n=4$	$r_c=16.97$ Å
$n=6$	$r_c=16.10$ Å
$n=8$	$r_c=15.71$ Å
$n=10$	$r_c=15.49$ Å
$n=\infty$	$r_c=14.70$ Å

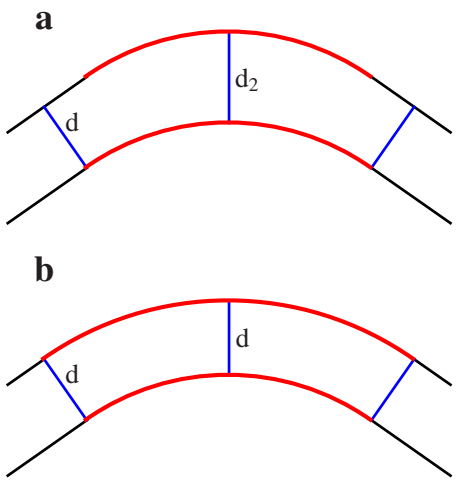

FIG. 9. (Color online) Two cases of how the radius of curvature changes for multiple nanotube layers. In (a) the radius of curvature remains constant, in (b) the radius of curvature increases by the interlayer spacing, d.

mations in this model and how they affect the critical radius.

The first issue to consider is the radius of curvature at the corners of the polygon and how this radius of curvature might change for multiple nanotube layers. The previous discussion and equations in this paper have assumed that the radius of curvature is the same for every layer of the nanotube. This implies that the interlayer spacing cannot be the same throughout the corner.

There are two extreme cases as to how the radius of curvature may change between successive layers. Either the radius of curvature is constant for every layer or the radius of curvature increases by the interlayer spacing every layer. Figure 9 illustrates these extremes. Figure 9(a) shows two layers where the radius of curvature is the same for each layer. In this case the interlayer spacing is larger at the corners than for the rest of the nanotube. The ratio of d_2 to d is $\frac{1}{\cos(\frac{\beta}{2})}$. For $\beta=60°$ this corresponds to a difference in interlayer spacing of 15%. Figure 9(b) shows two layers where the radius of curvature changes by the interlayer spacing from one layer to the next. In this case the spacing is the same at the corners as it is in the rest of the nanotube. However, when the radius of curvature increases, the curved length also increases. As a result the amount of incoherent interface increases with the radius of curvature. As we have no information on how the interfacial energy changes with an increase in the interlayer spacing we cannot predict which of the extremes is more likely.

Equations (9), (11), and (13) are derived under the assumption that the radius of curvature is constant. One can revise Eq. (9) to account for a different radius of curvature in each layer:

$$E_{\text{polygon}} = 2\pi C_{\text{length}} \sum_{i=0}^{n-1} \frac{C_{\text{bend}}}{r_c + id} + 2\pi\gamma_{\text{int}}\left[\left(r_c + \frac{d}{2}\right)(n-1) + d(n-2)\right]. \quad (14)$$

The variable r_c is the radius of curvature of the innermost layer. For several values of n Table III shows the radius of curvature of the innermost nanotube layer that results in the minimum energy.

TABLE III. Optimum radius of curvature for several values of the number of layers, n, for the case where the radius of curvature changes from one layer to the next.

Number of layers	Optimum r_c
2	18.4 Å
4	11.5 Å
6	8.8 Å
8	7.2 Å
10	6.2 Å

As can be seen from Table III, Eq. (9) does not change the main conclusion of this paper, above a critical radius, polygonal nanotubes have lower energy than circular nanotubes. In fact, the critical radius is lower in this case than for the original model. If the optimum radius of curvature is smaller than the radius of the innermost nanotube layer and the chirality of the nanotube is symmetrically equivalent to one of those shown in Table I, then the polygonal model will be the low-energy solution. Most inorganic nanotubes have approximately ten layers and an inner radius of 50 Å.[52,57,59,68] This is well above the optimum radius of curvature shown in either Table II or III, and hence it should be favorable for them to form polygons.

As mentioned in Sec. II, calculations discussed in this paper are for armchair nanotubes. Armchair nanotubes were chosen for extensive study because this chirality provides the smallest unit cell. Calculations were also performed on zigzag $(n,0)$ nanotubes for comparison. The bending strain energy constant and interfacial energy constant change with chirality, but the difference is not large enough to change the main conclusion of this paper. The dominant effect of chirality is that it determines the length of the lattice parameter in the rolling direction as discussed in Sec. III

Because the length of the periodic unit cell, which accounts for the difference in length between two consecutive corners, will rarely be equal to $2\Delta l$ from Eq. (12) there will be some tensile or compressive strain. Table I shows all of the chiralities for which the polygonal model applies and the fractional strain for each chirality. The strain fractions shown in Table I are calculated by dividing the difference between the unit cell length, a, and $2\Delta l$ by the length of the arc at the corner:

$$\epsilon = \frac{a - \beta d}{\beta r_c}. \quad (15)$$

The value of r_c used is the value shown in Table II for an infinite number of layers, 14.7 Å. The value of ϵ will decrease for larger radii of curvature and increase for smaller radii of curvature. The value of ϵ will also increase with multiple layers. The values shown in Table I apply to the second layer. For the third layer the strain will be twice as large, three times as large for the fourth layer, etc. This is essentially because the third layer will have two more peri-

odic units than the first layer, so the numerator of Eq. (15) will be twice as large, while the denominator will not change considerably. This strain must be considered. To quantify the magnitude of this strain we calculated the total tensile strain for a ten-layer nanotube with a chirality of (2,1), where the radius of curvature of consecutive layers increases by the interlayer spacing, as shown in Fig. 9(b). Equation (18) summarizes these calculations.

$$r_{\mathrm{ci}} = r_{c0} + d(i-1)[i = 1,2,3 \ldots 10], \tag{16}$$

$$\epsilon_i = \frac{(a - \beta d) \times (i-1)}{\beta r_{\mathrm{ci}}}, \tag{17}$$

$$\Delta E_i = 2\pi r_{\mathrm{ci}} C_{\mathrm{length}} C_{\mathrm{strain}} \epsilon_i^2. \tag{18}$$

The calculated tensile strain for the entire ten-layer nanotube is 183 meV, corresponding to 0.1 meV per strained atom. This is a negligible amount of strain energy, but this calculation is for the chirality with the smallest strain fraction. For a similar ten-layer nanotube with a chirality of (4,1), which has the largest strain fraction of all chiralities shown in Table I, the calculated tensile strain energy is 23.25 eV or 11.3 meV per strained atom. This is a considerable amount of strain energy and could prevent polygonal nanotube formation.

At this point there is limited experimental evidence of polygonal inorganic nanotubes. There are a few possible reasons for this. There are only a few examples of cross sectional images of nanotubes, so if polygonal nanotubes exist, it is unlikely they would be seen. There are many examples of faceted nanoparticles.[6,7,69] It is difficult to distinguish a very short nanotube from a nanoparticle. When a nanotube is faceted as in the polygonal model, it is possible that instead of nanotube growth, the ends of the nanotube close to form a very short, closed ended nanotube, which has the appearance of a nanoparticle. Reference 69 shows a CdI_2 nanoparticle with an hexagonal-cross section. The particle appears to be a polygonal nanotube that only grew to a length of 10 nm before closing at the ends.

Thus far polygonal nanotubes have been depicted in this paper as having a cross section that is a regular polygon, but this is not a requirement. Because all strain and interfacial energy is located in the corners, the length and location of the flat segments have no effect on the energy. Figure 10 illustrates this point. This figure shows two possible nanotube cross sections. In each case the curved length and radius of curvature of each corner are identical. The total length of the flat sections in each case is also identical. As a result each nanotube would have the same energy. This point is reinforced by Ref. 69. This paper shows two CdI_2 nanoparticles. The cross section of each nanoparticle is a hexagon, but the two hexagons are vastly different and neither one is a regular polygon. Due to this equivalence of structures, polygonal nanotubes can be distorted with no change in energy. There would be some force required to shift the position of the corners, but the initial and final structures will have the same energy. This only applies to open-ended nanotubes. The ends of closed-ended nanotubes would likely provide resistance to deformation.

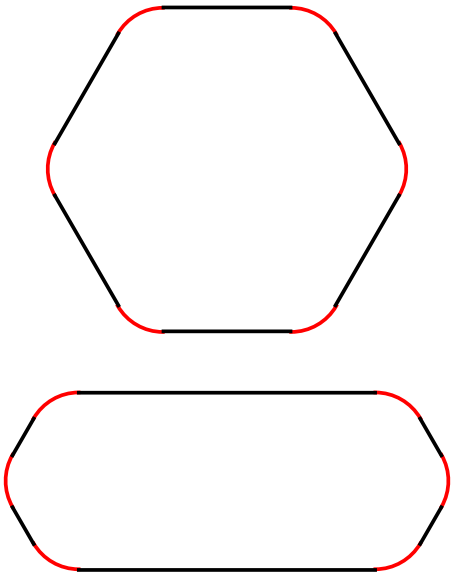

FIG. 10. (Color online) Cross section of two possible polygonal nanotubes that have the same energy in the polygonal model presented here

It is useful to consider how the radius of curvature required for polygonal nanotube formation varies with certain properties of the material. As is shown in Eq. (13), the optimum radius of curvature varies with the square root of the bending strain energy constant, so nanotubes of stiffer materials will require larger radii for polygonal nanotube formation. Stiffer materials will also have more tensile strain energy resulting from the mismatch between the lattice parameter and the excess length between layers, further reducing the likelihood of polygonal nanotube formation. The optimum radius of curvature varies inversely with the square root of the interfacial energy constant, so the likelihood of polygonal nanotube formation is increased for materials with a larger interfacial energy constant.

VII. CONCLUSIONS

We have shown here that a multiwalled nanotube with a polygonal-cross section can have a lower energy than a nanotube with a circular-cross section. The polygonal-cross section results in higher strain energy because the bending radius is smaller, but this can be more than compensated for by reduced interfacial energy. This energy reduction occurs because the flat sections of the nanotube can have a coherent interface with no tensile strain. A coherent interface has much lower energy than an incoherent interface. When the cross section is circular it is not possible to maintain a coherent interface without an excessive amount of tensile strain.

In order to maintain a coherent interface in the flat sections of a polygonal nanotube the difference in length between two layers must be equal to an integer number of

lattice parameters in the rolling direction. This lattice parameter is determined by the chirality of the nanotube and only a few nanotube chiralities can therefore easily form polygons. The radius of inorganic nanotubes seen experimentally is considerably above the minimum radius required for the polygonal model to apply, so inorganic nanotubes with the required chiralities may form polygonal-cross sections, though they do not need to be regular polygons. The energy is determined strictly by the radius of curvature of the corners of the polygon. This would result in extremely low resistance to deformation of polygonal nanotubes.

We hope that the model predictions made in this paper will inspire further experimental investigations into the shape of multiwalled nanotubes.

ACKNOWLEDGMENTS

This work was supported by the MRSEC Program of the National Science Foundation under Grant No. DMR 02-13282, by the Assistant Secretary for Energy Efficiency and Renewable Energy, Office of FreedomCAR, and Vehicle Technologies of the U.S. Department of Energy under Contract No. DE-AC02-05CH11231, with the Lawrence Berkeley National Laboratory. Additional computer resources were provided by the National Partnership for Advanced Computing Infrastructure (NPACI) at the San Diego Supercomputer Center.

*kjt@mit.edu
†redoe@mit.edu
‡gceder@mit.edu

[1] S. Iijima, Nature (London) **354**, 56 (1991).
[2] R. Tenne, M. Margulis, M. Genut, and G. Hodes, Nature (London) **360**, 444 (1992).
[3] L. Margulis, G. Salitra, R. Tenne, and M. Tallanker, Nature (London) **365**, 113 (1993).
[4] M. Nath and C. N. R. Rao, Angew. Chem., Int. Ed. **41**, 3451 (2002).
[5] C. N. R. Rao and Manashi Nath, Dalton Trans. **2003**, 1.
[6] R. Tenne, Chem.-Eur. J. **8**, 5296 (2002).
[7] M. Remskar, Adv. Mater. **16**, 1497 (2004).
[8] R. Tenne, J. Mater. Res. **21**, 2726 (2006).
[9] R. Tenne, Nat. Nanotechnol. **1**, 103 (2006).
[10] G. Tourillon, L. Pontonnier, J. P. Levy, and V. Langlais, Electrochem. Solid-State Lett. **3**, 20 (2000).
[11] N. Li, X. Li, X. Yin, W. Wang, and S. Qiu, Solid State Commun. **132**, 841 (2004).
[12] S. Iijima and T. Ichihashi, Nature (London) **363**, 603 (1993).
[13] M. Remskar, A. Mrzel, Z. Skraba, A. Jesih, M. Ceh, J. Demsar, P. Stadelmann, F. Levy, and D. Mihailovic, Science **292**, 479 (2001).
[14] Y. D. Li, X. L. Li, R. R. He, J. Zhu, and Z. X. Deng, J. Am. Chem. Soc. **124**, 1411 (2002).
[15] V. V. Ivanovskaya and G. Seifert, Solid State Commun. **130**, 175 (2004).
[16] Q. Chen, W. Zhou, G. Du, and L. M. Peng, Adv. Mater. **14**, 1208 (2002).
[17] W. Wang, O. K. Varghese, M. Paulose, and C. A. Grimes, J. Mater. Res. **19**, 417 (2004).
[18] R. Ma, Y. Bando, and T. J. Sasaki, J. Phys. Chem. B **108**, 2115 (2004).
[19] M. E. Spahr, P. Bitterli, R. Nesper, M. Muller, F. Krumeich, and H. U. Nissen, Angew. Chem., Int. Ed. **37**, 1263 (1998).
[20] Y. Maniwa *et al.*, Phys. Rev. B **64**, 073105 (2001).
[21] N. G. Chopra, R. J. Luyken, K. C. V. H. Crespi, M. L. Cohen, S. G. Louie, and A. Zettl, Science **269**, 966 (1995).
[22] L. Rapoport, N. Fleischer, and R. Tenne, J. Mater. Chem. **15**, 1782 (2005).
[23] A. Rothschild, S. R. Cohen, and R. Tenne, Appl. Phys. Lett. **75**, 4025 (1999).
[24] Y. Zhu, T. Sekine, K. Brigatti, S. Firth, R. Tenne, R. Rosentsveig, H. Kroto, and D. Walton, J. Am. Chem. Soc. **125**, 1329 (2003).
[25] G. Mor, M. Carvalho, O. Varghese, M. Pishko, and C. Grimes, J. Mater. Res. **19**, 628 (2004).
[26] M. Adachi, Y. Marata, I. Okada, and S. Yoshikawa, J. Electrochem. Soc. **150**, G488 (2003).
[27] Y. Lei, L. Zhang, G. Meng, G. Li, Z. Zhang, C. Liang, W. Chen, and S. Wang, Appl. Phys. Lett. **78**, 1125 (2001).
[28] F. Cheng and J. Chen, J. Mater. Res. **21**, 2744 (2006).
[29] J. Chen and F. Wu, Appl. Phys. A: Mater. Sci. Process. **78**, 989 (2004).
[30] J. Chen, Z. Tao, and S. Li, Angew. Chem., Int. Ed. **42**, 2147 (2003).
[31] Z. L. Tao, L. N. Xu, X. L. Gou, J. Chen, and H. T. Yuan, Chem. Commun. (Cambridge) **2004**, 2080.
[32] J. Chen, S. Li, Z. Tao, Y. Shen, and C. Cui, J. Am. Chem. Soc. **125**, 5284 (2003).
[33] R. Dominko, D. Arcon, A. Mrzel, Z. Zorko, P. Cevc, P. Venturini, and M. Gabe4rscek, M. Remskar, and D. Mihailovic, Adv. Mater. **14**, 1531 (2002).
[34] J. Chen, N. Kuriyama, H. Yuan, H. Takeshita, and T. Sakai, J. Am. Chem. Soc. **123**, 11813 (2001).
[35] D. V. Bavykin, A. A. Lapkin, P. K. Plucinsky, J. M. Friedrich, and F. C. Walsh, J. Phys. Chem. B **109**, 19422 (2005).
[36] Y. Zhou, L. Cao, F. Zhang, B. He, and H. Li, J. Electrochem. Soc. **150**, A1246 (2003).
[37] L. Jiao, H. Yuan, Y. Wang, J. Cao, and Y. Wang, Electrochem. Commun. **7**, 431 (2005).
[38] F. Y. Wu and H. M. Cheng, J. Phys. D **38**, 4302 (2005).
[39] M. Liu and J. M. Cowley, Carbon **32**, 393 (1994).
[40] M. Ishioka, T. Okada, K. Matsubara, M. Inagaki, and Y. Hishiyama, J. Mater. Res. **8**, 1866 (1993).
[41] C. H. Kiang, M. Endo, P. M. Ajayan, G. Dresselhaus, and M. S. Dresselhaus, Phys. Rev. Lett. **81**, 1869 (1998).
[42] D. Golberg, M. Mitome, Y. Bando, C. C. Tang, and C. Y. Zhi, Appl. Phys. A: Mater. Sci. Process. **88**, 347 (2007).
[43] A. Celik-Aktas, J. M. Zuo, J. F. Stubbins, C. Tang, and Y. Bando, Acta Crystallogr., Sect. A: Found. Crystallogr. **61**, 533 (2005).
[44] S. Dimovski and Y. Gogotsi, *Nanomaterials Handbook* (Taylor and Francis, London, 2007).

[45] J. S. Speck, M. Endo, and M. S. Dresselhaus, J. Cryst. Growth **94**, 834 (1989).
[46] Y. Gogotsi, J. A. Libera, N. Kalashnikov, and M. Yoshimura, Science **290**, 317 (2000).
[47] H. Okuno, A. Palnichenko, J. F. Despres, J. P. Issi, and J. C. Charlier, Carbon **43**, 692 (2005).
[48] N. G. Chopra, L. X. Benedict, V. H. Crespi, M. L. Cohen, S. G. Louie, and A. Zettl, Nature (London) **377**, 135 (1995).
[49] S. Iijima, C. Brabec, A. Maiti, and J. Bernhole, J. Chem. Phys. **104**, 2089 (1996).
[50] V. Lordi and N. Yao, J. Chem. Phys. **109**, 2509 (1998).
[51] U. D. Venkateswaran, A. M. Rao, E. Richter, M. Menon, A. Rinzler, R. E. Smalley, and P. C. Eklund, Phys. Rev. B **59**, 10928 (1999).
[52] U. Q. Zhu, W. K. Hsu, N. Grobert, B. H. Chang, M. Terrones, H. Terrones, G. W. Kroto, and D. R. M. Walton, Chem. Mater. **12**, 1190 (2000).
[53] Y. Q. Zhu *et al.*, J. Mater. Chem. **10**, 2570 (2000).
[54] J. C. Charlier, P. Lambin, and T. W. Ebbesen, Phys. Rev. B **54**, R8377 (1996).
[55] J. Tang, L. C. Qin, T. Sasaki, M. Yudasaka, A. Matsushita, and S. Iijima, Phys. Rev. Lett. **85**, 1887 (2000).
[56] S. F. Braga and D. S. Galvao, J. Comput. Chem. **28**, 1724 (2007).
[57] Y. Feldman, E. Wasserman, D. Srolovitz, and R. Tenne, Science **267**, 222 (1995).
[58] M. Nath and C. N. R. Rao, J. Am. Chem. Soc. **123**, 4841 (2001).
[59] J. Chen, S. L. Li, Z. L. Tao, and F. Gao, Chem. Commun. (Cambridge) **2003**, 980.
[60] J. P. Perdew, K. Burke, and Y. Wang, Phys. Rev. B **54**, 16533 (1996).
[61] P. E. Blochl, Phys. Rev. B **50**, 17953 (1994).
[62] G. Kresse and D. Joubert, Phys. Rev. B **59**, 1758 (1999).
[63] K. Tibbetts, C. R. Miranda, Y. S. Meng, and G. Ceder, Chem. Mater. **19**, 5302 (2007).
[64] Y.-S. Lee and N. Marzari, Phys. Rev. Lett. **97**, 116801 (2006).
[65] A. D. Yoffe, Solid State Ionics **39**, 1 (1990).
[66] V. V. Ivanovskaya, G. Seifert, and A. L. Ivanovskii, Semiconductors **39**, 1058 (2005).
[67] Y. S. Kim, M. Mizuno, I. Tanaka, and H. Adachi, Jpn. J. Appl. Phys., Part 1 **37**, 4878 (1998).
[68] A. Rothschild, G. L. Frey, M. Homyonfer, M. Rappaport, and R. Tenne, Mater. Res. Innovations **3**, 145 (1999).
[69] R. Popovitz-Biro, N. Sallacan, and R. Tenne, J. Mater. Chem. **13**, 1631 (2003).